NANO LETTERS

Letter

pubs.acs.org/NanoLett

A Vanadium Dioxide Metamaterial Disengaged from Insulator-to-Metal Transition

Young-Gyun Jeong,[†] Sanghoon Han,[‡] Jiyeah Rhie,[†] Ji-Soo Kyoung,[†] Jae-Wook Choi,[†] Namkyoo Park,[‡] Seunghun Hong,[§] Bong-Jun Kim,[∥] Hyun-Tak Kim,[∥,⊥] and Dai-Sik Kim*[,†]

[†]Department of Physics and Astronomy and Center for Atom Scale Electromagnetism, Seoul National University, Seoul 151-747, Republic of Korea

[‡]Photonic Systems Laboratory, School of EECS, Seoul National University, Seoul 151-744, Republic of Korea

[§]Department of Physics and Astronomy, Department of Biophysics and Chemical Biology, and Institute of Applied Physics, Seoul National University, Seoul 151-747, Republic of Korea

[∥]Creative Research Center of Metal−Insulator Transition, Electronics and Telecommunications Research Institute, Daejeon 305-700, Republic of Korea

[⊥]School of Advanced Device Technology, University of Science and Technology, Daejeon 305-333, Republic of Korea

Supporting Information

ABSTRACT: We report that vanadium dioxide films patterned with $\lambda/100000$ nanogaps exhibit an anomalous transition behavior at millimeter wavelengths. Most of the hybrid structure's switching actions occur well below the insulator to metal transition temperature, starting from 25 °C, so that the hysteresis curves completely separate themselves from their bare film counterparts. It is found that thermally excited intrinsic carriers are responsible for this behavior by introducing enough loss in the context of the radically modified electromagnetic environment in the vicinity of the nanogaps. This phenomenon newly extends the versatility of insulator to metal transition devices to encompass their semiconductor properties.

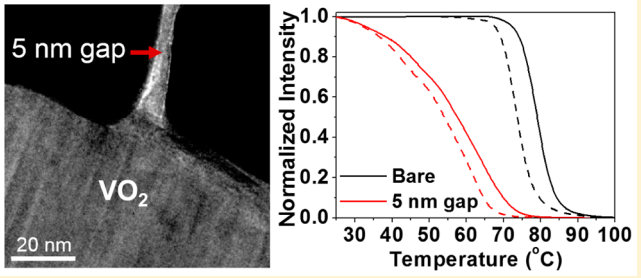

KEYWORDS: *Vanadium dioxide, insulator to metal transition, Boltzmann tail, nanogap, nano antenna, terahertz spectroscopy, transition device, lithography*

Phase transition phenomena have been one of the major issues of strongly correlated material researches. There have been a number of efforts to manipulate the transition properties of novel transition materials due to its wide potentials based on the drastic changes in optical, electronic, and structural properties.[1,2] In particular, some transition metal oxides such as vanadium oxides show the insulator-to-metal transition (IMT) behavior near room temperature, so that it can be a versatile material for temperature sensitive photonic and electronic devices.

Vanadium dioxide starts transiting from an insulator to a metallic state at around 68 °C. This transition can also be triggered by optical beams, electric fields, or external strains.[3−15] The lattice structure is transformed from monoclinic to tetragonal structures as the temperature rises, and the conductivity increases by several orders of magnitude during the transition (Figure 1a).[16] Because the transition temperature of VO_2 is at the highest end of the room-temperature range, there have been many approaches to lower it through doping, strain, substrates, and various fabrication techniques.[17−24] These attempts have been successful in lowering the transition temperature; however the overall modulation ranges of conductivity and optical responses suffer greatly.

In this work, we found a new approach toward engineering the apparent transition behavior in VO_2 without changing the material parameters themselves, simply by extreme nano-patterning (Figure 1b) tailored for millimeter wave applications. Having a semiconducting bandgap, even below the IMT temperature the number of electrons and holes keep increasing with temperature, with an $\exp\{-([E_g/(2k_BT)]\}$ (E_g, bandgap energy; k_B, Boltzmann constant; T, temperature (Kelvin)) dependence, although its influence to optical response is minimal. We manufactured a hybrid nanogap-VO_2 device entirely based upon this small change in dielectric constant, where the effective transition temperature is lowered by 20 degrees Celsius and the switching action starts more than 40 degrees earlier than in a bare film. Strikingly, the IMT part is not even needed for the device performance when an extreme nanogap is applied. Contrary to the chemical doping or

Received: April 1, 2015
Revised: August 17, 2015
Published: September 9, 2015

DOI: 10.1021/acs.nanolett.5b02361
Nano Lett. 2015, 15, 6318−6323

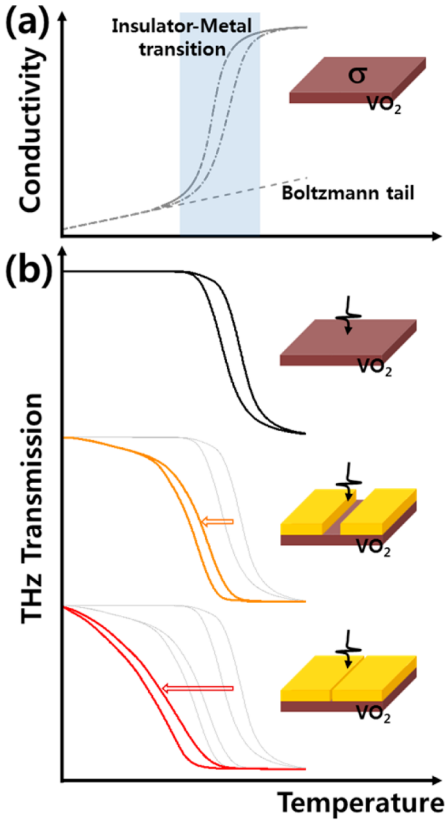

Figure 1. Insulator−metal transition of VO_2 film. (a) DC conductivity change of a VO_2 film in a logarithmic scale while the film is heated and cooled back (dash-dotted line). The conductivity drastically increases during the insulator-to-metal transition. The Boltzmann tail line (dotted) is an extension of conductivity changes by valence-to-conduction band thermal excitation before the insulator to metal transition. (b) Thermal hysteresis curves of THz transmission intensity on a bare VO_2 film (top) under the same thermal heating and cooling. (middle and bottom) Nanogap patterning pushes the hysteresis curves toward a lower temperature with a strong gap-width dependence.

mechanical strain modification for lowering the transition temperature in VO_2, the overall thermal transition behavior of our hybrid film device is determined by the width of the nanogap with high modulation range enhanced by at least 1 order of magnitude than the bare film.

Figure 2a displays the fabrication process of a nanogap-VO_2 hybrid structure. Our 100 nm thick VO_2 films were grown by the pulse laser deposition (PLD) method on a 430 μm thick *C*-plane sapphire substrate.[25] Conventional photolithography and atomic layer deposition are applied in 5 nm gap fabrication.[26] After cleaning the VO_2 film with acetone and isopropyl alcohol, a photoresist (AZ5206) is spin-coated and a UV beam is applied through a predesigned chrome mask which has a 25 μm × 25 μm square array with a 50 μm periodicity. A 250 nm thick first gold layer is evaporated and the photoresist pattern is lifted off. To improve the verticality of the structure and to remove the leftover photoresist, the structure is slightly milled by ion-beam so that the gold thickness becomes 200 nm. Though the ion-beam can in principle change the conductivity of VO_2 film, the effect is minimized in our sample because the ion beam mostly mills the tapered-edge gold layer and the leftover photoresist (Supporting Information Figure S1).

Once the first structure is ready, 5 nm thick Al_2O_3 oxide thin layer is deposited on the first gold layer by atomic layer deposition (ALD). After ALD, the second gold layer is deposited on top of the Al_2O_3 layer. In this case, there should not be any adhesion layer because the second gold layer deposited on the first gold layer has to be removed at the final stage. It is important to make discontinuity along the ring edges during the second layer deposition so that the part of the second layer deposited on the first layer can be removed. As the last process, we adopt commercial Scotch tape to peel off the part of the second layer deposited on the first surface.[26] If the taping is successful, 5 nm gaps can be formed at the edge of the 25 μm × 25 μm sized square rings (Figure 2b). A transmission electron microscopy (TEM) image of our final structure shows

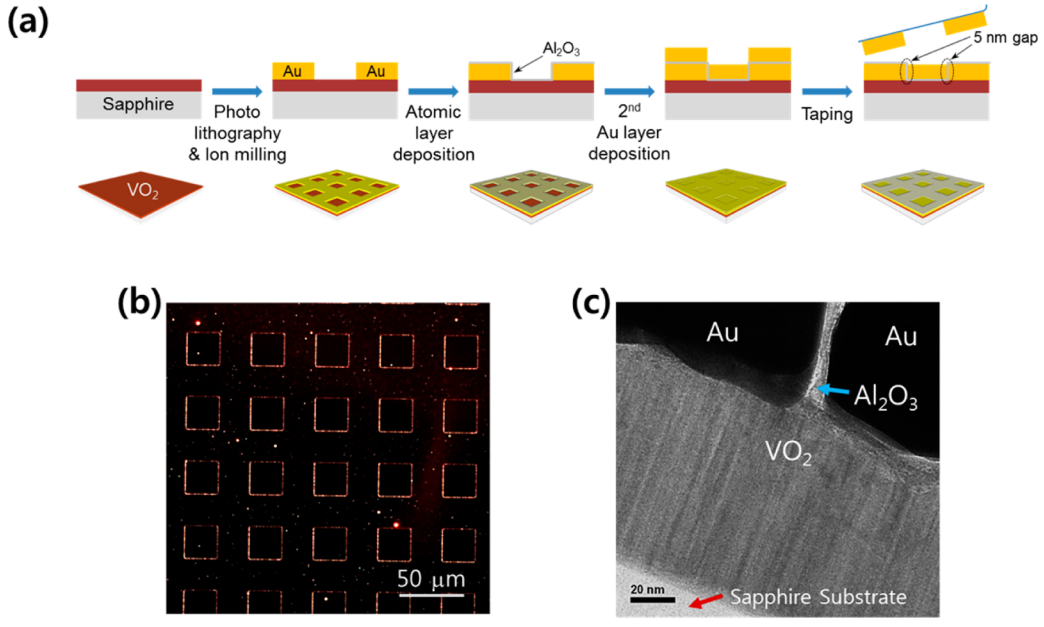

Figure 2. (a) Cross-section and top-view schematics of sample fabrication process. (b) Optical microscope image of a 25 μm × 25 μm sized 5 nm gap array. (c) Cross-section TEM image of a 5 nm gap fabricated on a 100 nm thick VO_2 film The left side gold is the first deposited layer.

DOI: 10.1021/acs.nanolett.5b02361
Nano Lett. 2015, 15, 6318−6323

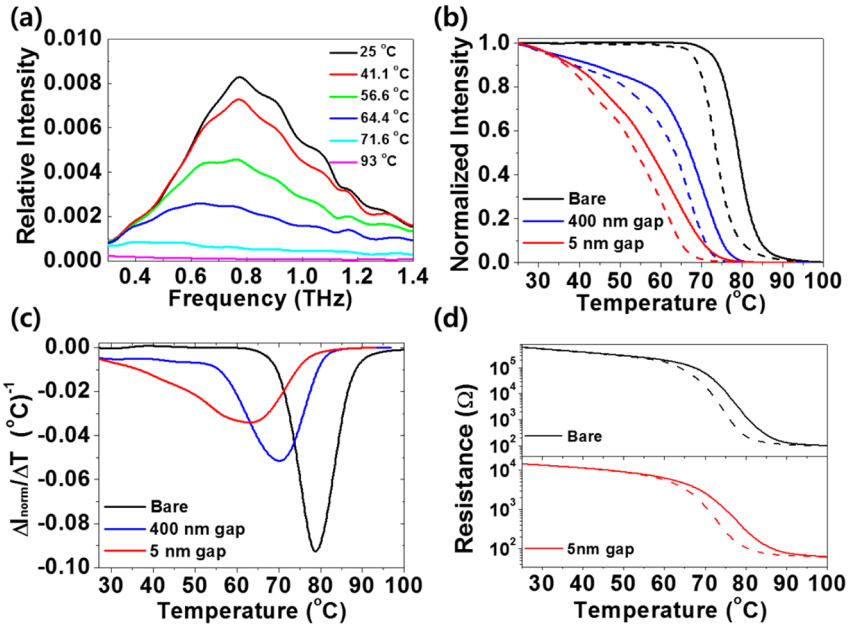

Figure 3. (a) Temperature-dependent THz transmission intensity spectra on 5 nm gap-VO_2 hybrid. (b) Thermal hysteresis curves of normalized THz transmission intensities for bare, 400, and 5 nm gap patterned VO_2 samples while heating (solid line) and cooling (dashed line). (c) Differentiated normalized intensity curves versus temperature (heating only). (d) Thermal hysteresis curves of electrical resistances for bare and 5 nm gap patterned VO_2 samples.

the hybrid junction of gold, Al_2O_3, and VO_2 in a 5 nm (Figure 2c).

Using terahertz (THz) time domain spectroscopy, we have measured THz transmission through a bare and nanogap patterned VO_2 hybrid film at different temperatures. Shown in Figure 3a are THz transmission intensity spectra divided by the transmission intensity of bare film for our 5 nm width square ring with resonance at 0.8 THz. At the resonance frequency, the modulation range of THz transmission intensity between 25 and 93 °C reaches 99% without any background signal subtraction. Though the relative transmission intensity of the nanogap patterned VO_2 film at room temperature is around 1% compared to the bare film, the modulation range is enhanced by 1 order of magnitude than the bare film so that the THz transmission can be fully switched off.

Now, we plot the temperature-dependent normalized THz transmission intensities of 5 and 400 nm gap samples at the resonance frequencies to compare with a bare film sample (Figure 3b). The 400 nm gap sample is fabricated by electron beam lithography with the same ring size and periodicity. Because of the difference of the gap width and the inside material of air versus Al_2O_3, the resonance frequency of the 400 nm gap sample is 1.3 THz.[27] We have normalized the maximum intensity with the minimum intensity offset to compensate the difference of absolute transmission intensities in each sample. In the heating process, THz transmission in a bare film starts to decrease around 70 °C due to the IMT of VO_2.[28,29]

On the contrary, when the 5 nm gap was patterned on the bare film, the THz transmission starts to decrease already from a room temperature, and the hysteresis curve is broad in the temperature range. While the film is heated, the normalized intensity essentially goes to zero at around 75 °C where the IMT is still unfinished and the bare film hysteresis barely starts. Though THz transmission on a bare VO_2 film is almost the same after heating and cooling, the hysteretic behavior of 5 nm gap patterned film is maintained even in the Boltzmann range because the nanogap is extremely sensitive to the electrical conductivity changes of VO_2 film. This means that the nanogap is able to detect the very small conductivity difference of VO_2 that originated from the persistent metallic domains in the insulating state after thermal IMT.[30−32] On the other hand, a reversible transition with virtually no hysteresis can be demonstrated when the temperature variation is confined within the Boltzmann tail range of less than 60 °C (Supporting Information Figure S2). When the gap width becomes larger, the hysteresis curve shifts more toward the bulk IMT as the 400 nm gap sample demonstrates.

When we compare the temperature derivatives of normalized transmission intensities ($\Delta I_{norm}/\Delta T$) in heating curves, our 5 nm gap hybrid film clearly shows a transiting behavior in the full temperature range while the bare film does not (Figure 3c). The 5 nm gap structure effectively amplifies the VO_2 functionality in that only a small variation of conductivity, which would have absolutely no effect on a bare film THz transmission, is enough to modulate the whole transmission rendering the IMT moot. The switching capability of our 5 nm gap-VO_2 hybrid film at around 30 °C with no chance for the IMT, represented by the derivative $\Delta I_{norm}/\Delta T$, is equivalent to the bare VO_2 at 65 °C, where the IMT is already well on the way.

In Figure 3d, we measure the temperature-dependent electrical resistances of bare and 5 nm gap patterned VO_2 films with two indium contacts separated by 1.8 cm on each film surface. Though the resistance of 5 nm gap patterned VO_2 film before the IMT is reduced by more than 1 order of magnitude due to the deposited metal layer between the contacts, the thermal hysteresis curves of resistances show a very similar transition range while the thermal hysteresis curves of THz transmission intensities on nanogap patterned VO_2 film shows distinct transition compared with a bare film. Also, the thermal hysteresis curves of femtosecond optical pulse

DOI: 10.1021/acs.nanolett.5b02361
Nano Lett. 2015, 15, 6318−6323

transmission for bare and nanoslot antenna patterned VO_2 film are almost overlapped (Supporting Information Figure S3). These results support that the transition temperature that determines the slope of thermal resistance curve in the Boltzmann tail regime are maintained after nanogap patterning.[9] The separation of thermal hysteresis curves of THz transmission is specific in functional resonance frequency range of THz nanogap structures, where the energy funneling is significant.

To investigate the gap width dependence in THz transition behavior of nanogap-VO_2 hybrid, we fabricate rectangular slot antenna array structures with electron beam lithography and measure THz transmission signals.[8] Figure 4a represents the sample schematic and an SEM image of a 180 nm width single nanoantenna. Total area of the nanoantenna array is 2 cm × 2 cm and the length of each antenna is 150 μm. The nearest two antennas are separated by 10 μm in the length direction and 30 μm in the width direction.

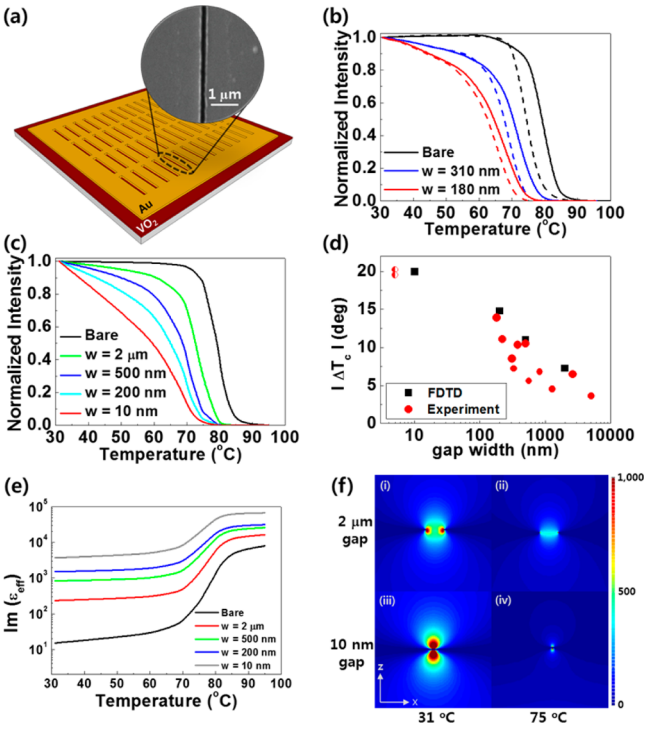

Figure 4. (a) Schematic of a slot antenna array patterned VO_2 hybrid sample and an SEM image of a 180 nm width nanoslot antenna. (b) Thermal hysteresis curves of normalized THz transmission intensities for bare, 310, and 180 nm width nanoslot antenna array patterned VO_2 films. The "w" means the width of nanoantennas. (c) FDTD simulation results of normalized THz transmission intensities for bare and nanoantenna patterned VO_2 with various antenna widths. (d) Transition temperature difference between a bare film and nanoslot antenna patterned films. FDTD simulations (black squares) together with experimental results (red circles). (e) Imaginary part of effective dielectric constants obtained from the FDTD result. (f) THz electric field intensity distribution on (i) 2 μm gap/VO_2 at 31 °C and (ii) 75 °C, and (iii) 10 nm gap/VO_2 at 31 °C and (iv) 75 °C.

We compare thermal hysteresis curves of THz transmission intensities in 180 and 310 nm width slot antenna arrays patterned VO_2 film, and a bare film. We heat the samples from 30 to 100 °C and cool it down back. To compare hysteresis behaviors among them in Figure 4b we plot temperature-dependent normalized THz transmission intensities at 0.4 THz, which is the resonance frequency of the 150 μm long slot antenna. We use the same normalization process as the 5 nm gap case. When the 180 nm width nanoantenna array is patterned on a bare film, the THz transmission starts to decrease from 30 °C and the hysteresis curve shows much lower effective transition temperature, defined as the midpoint of the normalized intensity. The transition curve of the 310 nm width sample lies between the bare and the 180 nm width sample. This result is consistent with the ring type nanogap experiments.

As a theoretical approach, we compute temperature dependent normalized THz transmission intensities during heating process with the finite-difference time-domain (FDTD) method for a resonance frequency-equivalent single-slot antenna structure, assuming bulk dielectric constants from earlier works (Figure 4c).[16,33−37] The hysteresis curve shift is well reproduced, including the gap width dependence. In FDTD calculation, the antenna widths vary from 2 μm to 10 nm. The FDTD results show that the transition starts in the Boltzmann tail range in nanoslot antenna array-patterned VO_2 samples despite using the same bulk VO_2 parameter; the narrower the antenna width, the lower the transition temperature.

To compare the FDTD calculation with experimental results, we measure various slot antenna width cases. The width of nanoantennas was varied between 180 nm and 5 μm with other parameters fixed. We display the gap width-dependence of the transition temperature, defined as the average of the half-point of the hysteresis curves of the heating and the cooling processes. $|\Delta T_c|$ is the difference between transition temperatures of bare and nanoantenna-patterned films (Figure 4d). Overall tendency from experiments and FDTD calculations using dielectric constants of bulk VO_2 shows clear correlations between the gap width and the transition temperature shift, including our 5 nm gap samples (half-filled red circles). This result shows that our nanogap structure can effectively modulate the thermal transition of THz transmission on VO_2 by 20 degrees.

We now compute, from the FDTD results, the effective dielectric constants of the nanoantenna array-patterned VO_2 films as a function of temperature. We assume a homogeneous medium of 100 nm thickness and back-calculate the dielectric constants that give the same amplitude-phase of the transmitted signal through the hybrid films.[38] Shown in Figure 4e are the imaginary parts of the effective dielectric constant as we vary the antenna width. In the 10 nm case, the constants are more than 2 orders of magnitude enhanced in Boltzmann tail range, so that the performance is equivalent to that of the metallic state of bare film. Our results suggest a remarkable potential to engineer the effective dielectric constants of the metal nanostructure-VO_2 composite, possibly up to the limit of the metal itself, at ambient temperatures.

For spatial analysis, we compare the vertical field profiles of a 2 μm gap (Figure 4f(i), (ii)) and a 10 nm gap (Figure 4f(iii), (iv)) respectively, at 31 and 75 °C. In the 10 nm gap sample, the funneling field is almost completely switched off at 75 °C while the transmission is still significant in the 2 μm gap, consistent with our experimental results. The transmitting THz wave experiences the conductivity changes of VO_2 much more sensitively because the nanogap structure introduces very unusual electromagnetic environment whereby the electric field is strongly enhanced where the magnetic field remains more or less the same. This new environment renormalizes the cross

DOI: 10.1021/acs.nanolett.5b02361
Nano Lett. 2015, 15, 6318−6323

section of the underlying VO_2 so that the imaginary part of the dielectric constant at 30 °C, which could not affect the transmission through a bulk VO_2 at all, still changes THz transmission appreciably.[27,39,40]

In conclusion, armed only with conventional photolithography and atomic layer deposition methods, we successfully fabricated negative square ring array structures of hybrid nanogap-strongly correlated systems. In a 5 nm gap-VO_2 hybrid film structure, we demonstrated a transition engineering by utilizing the Boltzmann tail of semiconducting VO_2 at an extreme subwavelength regime. Strikingly, the transmitting THz electromagnetic wave can be fully controlled before the IMT ever becomes prominent. We can engineer the onset of the apparent transition temperature by simply controlling the width of the nanogap. When we consider the generality of this phenomenon in VO_2 films (Supporting Information Figure S4), the transition temperature is expected to be further lowered in combination with other techniques such as doping, external strain, and substrate matching. These results will provide a wide potential in developing near room-temperature phase transition devices combined with plasmonic nanostructures.

■ ASSOCIATED CONTENT

Supporting Information

The Supporting Information is available free of charge on the ACS Publications website at DOI: 10.1021/acs.nanolett.5b02361.

The effect of ion-milling, hysteresis property, optical transmission property, and generality of the nanogap induced thermal hysteresis shift of THz transmission. (PDF)

■ AUTHOR INFORMATION

Corresponding Author

*E-mail: dsk@phya.snu.ac.kr.

Present Address

(J.-S.K.) Samsung Advanced Institute of Technology, Samsung Electronics Co., Suwon 443-803, Republic of Korea.

Author Contributions

Y.-G.J. and S.H. contributed equally.

The manuscript was written through contributions of all authors. All authors have given approval to the final version of the manuscript.

Notes

The authors declare no competing financial interest.

■ ACKNOWLEDGMENTS

The authors would like to thank Dr. Byoung-Chul Min for the support in ion-beam milling. This work was supported by the National Research Foundation of Korea (NRF) grant funded by the Korea government (MSIP: 2008-0061906, 2005-0093838, 2008-00580, 2014-004023, K20815000003, 2015R1A3A2031768) (MOE: BK21 Plus Program-21A20131111123) and the creative research project of ETRI.

■ REFERENCES

(1) Imada, M.; Fujimori, A.; Tokura, Y. *Rev. Mod. Phys.* **1998**, *70*, 1039−1263.

(2) Yang, Z.; Ko, C.; Ramanathan, S. *Annu. Rev. Mater. Res.* **2011**, *41*, 337−367.

(3) Cavalleri, A.; Tóth, C.; Siders, C. W.; Squier, J. A.; Ráksi, F.; Forget, P.; Kieffer, J. C. *Phys. Rev. Lett.* **2001**, *87*, 2374011−2374014.

(4) Kim, H.-T.; Chae, B.-G.; Youn, D.-H.; Maeng, S.-L.; Kim, G.; Kang, K.-Y.; Lim, Y.-S. *New J. Phys.* **2004**, *6*, 52.

(5) Wei, J.; Wang, Z.; Chen, W.; Cobden, D. H. *Nat. Nanotechnol.* **2009**, *4*, 420−424.

(6) Nakano, M.; Shibuya, K.; Okuyama, D.; Hatano, T.; Ono, S.; Kawasaki, M.; Iwasa, Y.; Tokura, Y. *Nature* **2012**, *487*, 459−462.

(7) Liu, M.; Hwang, H. Y.; Tao, H.; Strikwerda, A. C.; Fan, K.; Keiser, G. R.; Sternbach, A. J.; West, K. G.; Kittiwatanakul, S.; Lu, J.; Wolf, S. A.; Omenetto, F. G.; Zhang, X.; Nelson, K. A.; Averitt, R. D. *Nature* **2012**, *487*, 345−348.

(8) Seo, M.; Kyoung, J.; Park, H.; Koo, S.; Kim, H.-S.; Bernien, H.; Kim, B. J.; Choe, J. H.; Ahn, Y. H.; Kim, H.-T.; Park, N.; Park, Q. H.; Ahn, K.; Kim, D.-S. *Nano Lett.* **2010**, *10*, 2064−2068.

(9) Driscoll, T.; Kim, H.-T.; Chae, B.-G.; Kim, B.-J.; Lee, Y.-W.; Jokerst, N. M.; Palit, S.; Smith, D. R.; Di Ventra, M.; Basov, D. N. *Science* **2009**, *325*, 1518−1521.

(10) Jones, A. C.; Berweger, S.; Wei, J.; Cobden, D.; Raschke, M. B. *Nano Lett.* **2010**, *10*, 1574−1581.

(11) Sohn, J. I.; Joo, H. J.; Ahn, D.; Lee, H. H.; Porter, A. E.; Kim, K.; Kang, D. J.; Welland, M. E. *Nano Lett.* **2009**, *9*, 3392−3397.

(12) Arcangeletti, E.; Baldassarre, L.; Di Castro, D.; Lupi, S.; Malavasi, L.; Marini, C.; Perucchi, A.; Postorino, P. *Phys. Rev. Lett.* **2007**, *98*, 196406.

(13) Kim, J.; Ko, C.; Frenzel, A.; Ramanathan, S.; Hoffman, J. E. *Appl. Phys. Lett.* **2010**, *96*, 213106.

(14) Guo, H.; Chen, K.; Oh, Y.; Wang, K.; Dejoie, C.; Syed Asif, S. A.; Warren, O. L.; Shan, Z. W.; Wu, J.; Minor, A. M. *Nano Lett.* **2011**, *11*, 3207−3213.

(15) Zimmers, A.; Aigouy, L.; Mortier, M.; Sharoni, A.; Wang, S.; West, K. G.; Ramirez, J. G.; Schuller, I. K. *Phys. Rev. Lett.* **2013**, *110*, 056601.

(16) Hilton, D. J.; Prasankumar, R. P.; Fourmaux, S.; Cavalleri, A.; Brassard, D.; Khakani, M. A. E.; Kieffer, J. C.; Taylor, A. J.; Averitt, R. D. *Phys. Rev. Lett.* **2007**, *99*, 226401.

(17) Booth, J. M.; Casey, P. S. *Phys. Rev. Lett.* **2009**, *103*, 086402.

(18) Jin, P.; Nakao, S.; Tanemura, S. *Thin Solid Films* **1998**, *324*, 151−158.

(19) Soltani, M.; Chaker, M.; Haddad, E.; Kruzelecky, R. V.; Margot, J. *Appl. Phys. Lett.* **2004**, *85*, 1958−1960.

(20) Lopez, R.; Feldman, L. C.; Haglund, R. F., Jr *Phys. Rev. Lett.* **2004**, *93*, 177403.

(21) Chen, S.; Ma, H.; Dai, J.; Yi, X. *Appl. Phys. Lett.* **2007**, *90*, 101117−3.

(22) Jeong, J.; Aetukuri, N.; Graf, T.; Schladt, T. D.; Samant, M. G.; Parkin, S. S. P. *Science* **2013**, *339*, 1402−1405.

(23) Cao, J.; Ertekin, E.; Srinivasan, V.; Fan, W.; Huang, S.; Zheng, H.; Yim, J. W. L.; Khanal, D. R.; Ogletree, D. F.; Grossman, J. C.; Wu, J. *Nat. Nanotechnol.* **2009**, *4*, 732−737.

(24) Wen, Q.-Y.; Zhang, H.-W.; Yang, Q.-H.; Xie, Y.-S.; Chen, K.; Liu, Y.-L. *Appl. Phys. Lett.* **2010**, *97*, 021111.

(25) Kim, D. H.; Kwok, H. S. *Appl. Phys. Lett.* **1994**, *65*, 3188−3190.

(26) Chen, X.; Park, H.-R.; Pelton, M.; Piao, X.; Lindquist, N. C.; Im, H.; Kim, Y. J.; Ahn, J. S.; Ahn, K. J.; Park, N.; Kim, D.-S.; Oh, S.-H. *Nat. Commun.* **2013**, *4*, 2361.

(27) Park, H. R.; Koo, S. M.; Suwal, O. K.; Park, Y. M.; Kyoung, J. S.; Seo, M. A.; Choi, S. S.; Park, N. K.; Kim, D. S.; Ahn, K. J. *Appl. Phys. Lett.* **2010**, *96*, 211109−3.

(28) Pashkin, A.; Kübler, C.; Ehrke, H.; Lopez, R.; Halabica, A.; Haglund, R. F.; Huber, R.; Leitenstorfer, A. *Phys. Rev. B: Condens. Matter Mater. Phys.* **2011**, *83*, 195120.

(29) Nakajima, M.; Takubo, N.; Hiroi, Z.; Ueda, Y.; Suemoto, T. *Appl. Phys. Lett.* **2008**, *92*, 011907.

(30) Suh, J. Y.; Lopez, R.; Feldman, L. C.; Haglund, R. F. *J. Appl. Phys.* **2004**, *96*, 1209−1213.

(31) Ramírez, J. G.; Sharoni, A.; Dubi, Y.; Gómez, M. E.; Schuller, I. K. *Phys. Rev. B: Condens. Matter Mater. Phys.* **2009**, *79*, 235110.

(32) Qazilbash, M. M.; Brehm, M.; Andreev, G. O.; Frenzel, A.; Ho, P. C.; Chae, B.-G.; Kim, B.-J.; Yun, S. J.; Kim, H.-T.; Balatsky, A. V.;

DOI: 10.1021/acs.nanolett.5b02361
Nano Lett. 2015, 15, 6318−6323

Shpyrko, O. G.; Maple, M. B.; Keilmann, F.; Basov, D. N. *Phys. Rev. B: Condens. Matter Mater. Phys.* **2009**, *79*, 075107.
(33) Kübler, C.; Ehrke, H.; Huber, R.; Lopez, R.; Halabica, A.; Haglund, R. F.; Leitenstorfer, A. *Phys. Rev. Lett.* **2007**, *99*, 116401.
(34) Cocker, T. L.; Titova, L. V.; Fourmaux, S.; Bandulet, H. C.; Brassard, D.; Kieffer, J. C.; El Khakani, M. A.; Hegmann, F. A. *Appl. Phys. Lett.* **2010**, *97*, 221905−3.
(35) Jepsen, P. U.; Fischer, B. M.; Thoman, A.; Helm, H.; Suh, J. Y.; Lopez, R.; R. F. Haglund, J. *Phys. Rev. B: Condens. Matter Mater. Phys.* **2006**, *74*, 205103.
(36) Qazilbash, M. M.; Brehm, M.; Chae, B.-G.; Ho, P.-C.; Andreev, G. O.; Kim, B.-J.; Yun, S. J.; Balatsky, A. V.; Maple, M. B.; Keilmann, F.; Kim, H.-T.; Basov, D. N. *Science* **2007**, *318*, 1750−1753.
(37) Mandal, P.; Speck, A.; Ko, C.; Ramanathan, S. *Opt. Lett.* **2011**, *36*, 1927−1929.
(38) Kyoung, J. S.; Seo, M. A.; Koo, S. M.; Park, H. R.; Kim, H. S.; Kim, B. J.; Kim, H. T.; Park, N. K.; Kim, D. S.; Ahn, K. J. *Phys. Status Solidi C* **2011**, *8*, 1227−1230.
(39) Park, H.-R.; Ahn, K. J.; Han, S.; Bahk, Y.-M.; Park, N.; Kim, D.-S. *Nano Lett.* **2013**, *13*, 1782−1786.
(40) Adato, R.; Artar, A.; Erramilli, S.; Altug, H. *Nano Lett.* **2013**, *13*, 2584−2591.

DOI: 10.1021/acs.nanolett.5b02361
Nano Lett. 2015, 15, 6318−6323